RESEARCH ARTICLE

NANO · MICRO small
www.small-journal.com

Remotely Sequential Activation of Biofunctional MXenes for Spatiotemporally Controlled Photothermal Cancer Therapy Integrated with Multimodal Imaging

*Jing Jia, Xiaobo Zhang, Yiran Li, Tian Wang, Ying An, Xinrong Yan, Bin Liu, Chaoyi Yang, and Huangxian Ju**

Spatiotemporally controlled cancer therapy may offer great advantages in precision medicine, but still remains some challenges in programmed sequential release and co-localization of components at target sites. Herein, a MXene-based nanoprobe (TCC@M) is meticulously designed by engineering of photodynamically activated CRISPR-Cas9 and cancer cell membrane-camouflaged Ti_3C_2 MXenes for targeting delivery and spatiotemporally controlled gene regulation followed by enhanced photothermal therapy (PTT) via two near-infrared irradiations. The first irradiation can activate the photosensitizer bound in cancer cells internalized TCC@M to release Cas9 ribonucleoprotein (RNP) by photodynamic effect. The released Cas9 RNP then enters the nuclei directed by the fused nuclear localization sequence in Cas9 to cleave the heat shock protein (HSP) 90α gene, which greatly reduces the expression of HSP90α protein and thus effectively sensitizes cancer cells to heat, leading to enhanced PTT at a mild temperature (<45 °C) risen by Ti_3C_2 MXenes under the second irradiation. Simultaneously, TCC@M can produce fluorescence, photoacoustic, and thermal imaging signals to guide the optimal irradiation timing. The in vivo studies have demonstrated the spatiotemporally selective therapeutic efficacy of the designed TCC@M. This innovative approach presents an effective integration of gene regulation and enhanced PTT, exemplifying a precise cancer treatment strategy.

1. Introduction

Multi-synergistic platforms are frequently exploited for more effective cancer treatment, considering the complex and dynamic physicochemical environment in vivo.[1] However, traditional cocktail-based combination therapies encounter great challenges in synergy due to differences in pharmacokinetics and sites of action. Careful manipulation of dosing regimens, particularly through the sequential activation of combination treatments, can achieve high spatial or temporal selectivity in drug delivery, creating a more precise therapeutic environment.[2] Smart drug delivery systems that respond to external[3] or internal[4] stimuli have been designed to optimize the timing and location of therapeutic onset. Additionally, therapeutic agents are often administered with sensitizers to enhance treatment efficacy.[5] For instance, heat-based therapies are commonly combined with heat shock protein (HSP) inhibitors to overcome the resistance mediated by HSP upregulation in response to cellular stress, particularly elevated temperatures.[6] By downregulating HSP expression, this strategy improves therapeutic efficacy in the targeted region.[7] However, the majority of these strategies offer the control in only temporal or spatial dimension and often lack real-time tracking capabilities to monitor the treatment effects. Additionally, endogenous stimuli may inadvertently trigger responses in neighboring non-tumor tissues due to the complex nature of the tumor microenvironment (TME).[8] Furthermore, therapeutic inhibitory molecules such as HSPs are essential for normal cellular functions, including proper protein folding and protection against external stressors.[9] Therefore, the design of theranostic strategies that integrate spatiotemporally controlled therapy with real-time imaging is still urgent needs for offering a precise and effective approach to cancer treatment.[10]

Light-controlled gene regulation has attracted significant attention in cancer treatment and early diagnosis due to its exceptional spatiotemporal controllability.[11] Nevertheless, reliance on ultraviolet (UV) light or optogenetic engineering in these systems presents limitations in clinical application, including poor tissue penetration and the need for complex technologies. Although upconversion nanoparticles have been developed to convert near-infrared (NIR) light into UV emissions,[12] these systems lack the capacity to selectively adjust power output between tumor and normal cells in the complex TME, owing to their dependence on exogenous modulation. To overcome these drawbacks,

J. Jia, X. Zhang, Y. Li, T. Wang, Y. An, X. Yan, B. Liu, C. Yang, H. Ju
State Key Laboratory of Analytical Chemistry for Life Science
School of Chemistry and Chemical Engineering
Nanjing University
Nanjing 210023, China
E-mail: hxju@nju.edu.cn

The ORCID identification number(s) for the author(s) of this article can be found under https://doi.org/10.1002/smll.202410535

DOI: 10.1002/smll.202410535

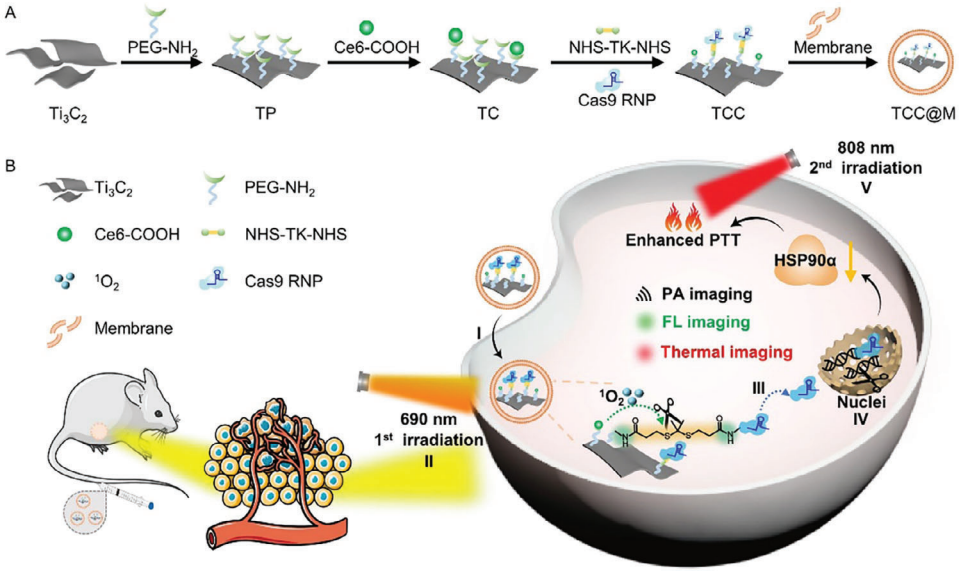

Scheme 1. General design of nano-theranostic TCC@M with light-controlled sequential activation. (A) Schematic illustration of TCC@M preparation. (B) Sequential irradiation to activate TCC@M for enhanced PTT and multimodal imaging. (I) Transfection of TCC@M into the cell. (II) The first irradiation of Ce6 to produce $^1O_2$. (III) TK cleavage by $^1O_2$ to release Cas9 RNP. (IV) Degradation of HSP90α gene by Cas9 RNP in nuclei. (V) Enhanced PTT under the second irradiation along with multimodal imaging.

in this study we developed a MXene-based nanoprobe (TCC@M) by integrating the advanced nanocarrier and gene technologies to achieve light-controlled sequential activation of gene regulation and enhanced photothermal therapy (PTT) along with multimodal imaging (**Scheme 1**).

Ti_3C_2 MXenes have been known for their strong light absorption in the NIR region and high photothermal conversion efficiency.[13,14] Despite their potential for deep tissue PTT and photoacoustic imaging in NIR region,[15] conventional hyperthermia (>50 °C) and instability under physiologic conditions limit their clinical application. Here, Ti_3C_2 MXenes were utilized as both the vector of Cas9 ribonucleoprotein (RNP) and photosensitizer chlorin e6 (Ce6) for performing gene regulation with clustered regularly interspaced short palindromic repeats (CRISPR) technology[16] and the photothermal therapeutic agents for achieving enhanced cancer treatment. By camouflaging the biofunctional MXenes (TCC) with cancer cell membranes (CCMs) (Scheme 1A), the tumor site accumulation and targeting delivery of TCC@M into tumor cells were successfully achieved due to the homology targeting effect.[17] After the first irradiation to activate the photodynamic effect of Ce6 for releasing Cas9 RNP, the released Cas9 RNP could entered the nuclei by the fused nuclear localization sequence in Cas9 to cleave HSP90α DNA targeted by single guide RNAs (sgRNAs), which greatly reduced the expression of HSP90α protein to effectively sensitize cancer cells to heat, leading to enhanced subsequent PTT of MXenes (Scheme 1B). Followed with the second irradiation, the PTT could be performed at a mild temperature (<45 °C). Furthermore, the presence of Ce6 and MXenes provided respectively fluorescence (FL) and photoacoustic (PA) as well as thermal signals under two irradiations, which led to a multimodal imaging approach to guide the optimal irradiation timing. As a proof-of-concept, A549 tumor-bearing nude mice were used as the model to receive intravenous injections, which demonstrated the practicability of the remotely sequential activation of biofunctional MXenes in precision and highly effective cancer therapy.

2. Results and Discussion

2.1. Characterization of TCC@M

As a star member of the MXenes family, Ti_3C_2 nanosheets (NSs) with a 2D structure were synthesized using an in situ HF etching method followed by sonication.[18] The obtained Ti_3C_2 NSs showed a sheet morphology (Figure S1A, Supporting Information) with an average hydrodynamic size of 93.2 nm (**Figure 1A**), which was a suitable size for cell uptake. The successful preparation of monolayer Ti_3C_2 was also confirmed by XRD and UV absorption spectra (Figure S2, Supporting Information), which exhibited broad and intense absorption with the maximum wavelength at 760 nm and a molar extinction coefficient of 20.0 g^{-1} L cm^{-1}. The relatively negative Zeta potential of Ti_3C_2 NSs (Figure 1A) indicated the presence of surface -OH and -F groups,[19] which led to convenient assembly of positively charged 4-armed PEG-NH_2 to produce PEG functionalized Ti_3C_2 (TP) for covalently binding Ce6 to attain TC and then Cas9 RNP in the presence of NHS-TK-NHS to obtain TCC (Scheme 1A). The TCC@M was thus prepared by mixing the obtained TCC and the extracted cell membranes to extrude through a polycarbonate membrane with 400 nm pore size. The Zeta potential exhibited an initial increase followed by decrease, whereas the size consistently increased with the sequential modifications of PEG-NH_2, Ce6, and Cas9 RNP on Ti_3C_2 NSs (Figures 1A and S1, Supporting Information). After Ce6 binding the formed TC showed the characteristic peaks of Ce6 in 450–750 nm, which could be remained

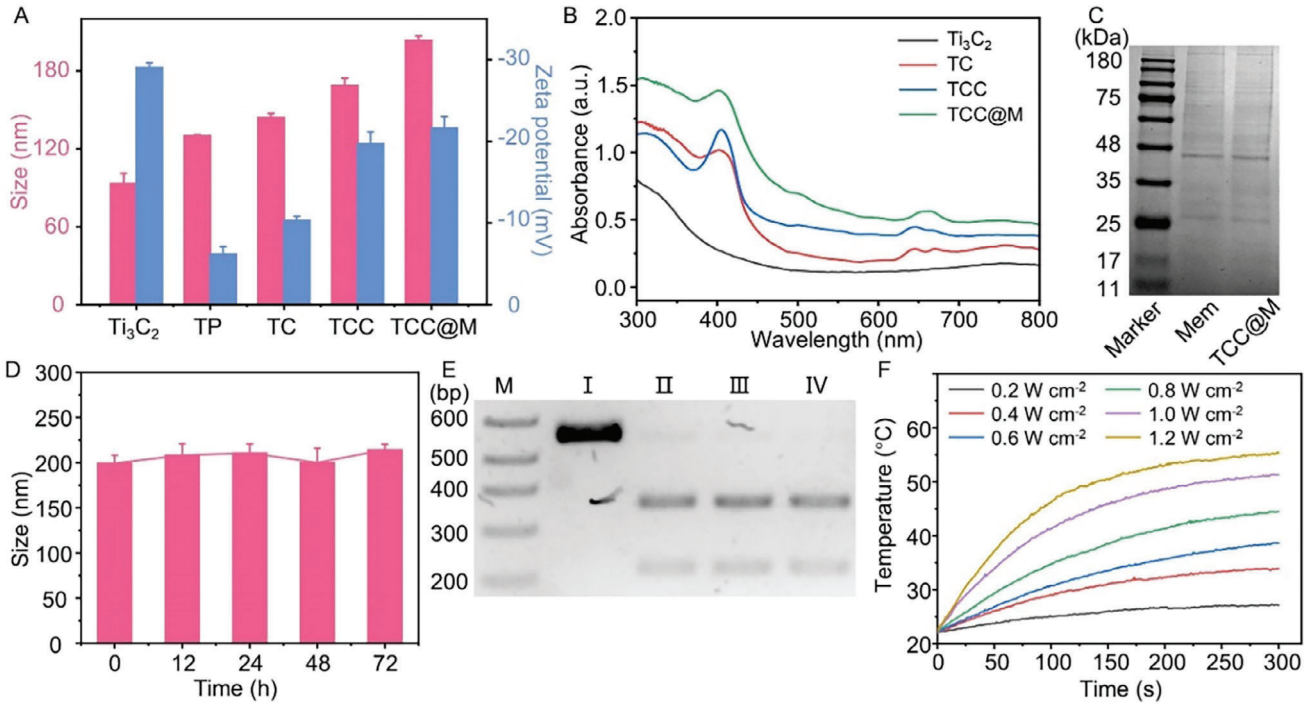

Figure 1. Characterization of TCC@M. (A) Hydrodynamic sizes and Zeta potentials of Ti_3C_2, TP, TC, TCC, and TCC@M. (B) Absorption spectra of Ti_3C_2, TC, TCC, and TCC@M. (C) SDS-PAGE protein analysis of A549 cell membrane and TCC@M. (D) Size change of TCC@M in water over 72 h. The data error bars represent mean ± SD ($n = 3$). (E) Gel electrophoresis of (I) HSP90α DNA, (II) the mixture of HSP90α DNA and Cas9 RNP, and (III, IV) the mixture of HSP90α DNA and TCC@M before (III) and after (IV) 690 nm irradiation. (F) Temperature change of TCC@M solution (50 μg mL^{-1}) under 808 nm irradiation with different power densities.

after cell membrane enveloping (Figure 1B), ensuring the photodynamic activation and FL signal.

The extracted Cas9 protein possessed a molecular weight of ≈160 kD along with the activity to degrade HSP90α DNA after conjugation with RNP, which led to a new PAGE band at low weight (Figure S3, Supporting Information). The successful binding of Cas9 RNP to TC was confirmed by SDS-

PAGE analysis of TCC, which indicated its good stability against 20 min centrifugation (14 000 rpm) (Figure S4, Supporting Information). SDS-PAGE protein analysis of A549 cell membrane and TCC@M displayed the same distribution of membrane proteins (Figure 1C), validating the success cell membrane enveloping. Moreover, the TCC@M showed good stability in water (Figure 1D), and the activity of Cas9 RNP in TCC@M did not also change upon cell membrane enveloping of TCC and 690 nm irradiation (Figure 1E), which showed the disappearance of HSP90α DNA band at 548 bp and the same bands of degraded HSP90α DNA at 352 and 196 bp, as that of free Cas9 RNP.

Ti_3C_2 NSs have been considered as a promising material for photothermal therapy and dual-modal imaging with a photothermal conversion of 30.6%.[20] After Cas9 RNP modification and cell membrane enveloping, the TCC@M retained considerable photothermal feature under 808 nm irradiation, which led to both power density- and concentration-dependent temperature rising of the irradiated TCC@M solution (Figures 1F and S5A, Supporting Information). Moreover, the temperature rising feature could be repeatedly observed upon cyclic irradiation and 3 irradiations at 24, 48, and 72 h (Figure S5B,C, Supporting Information), indicating good stability of photothermal conversion.

The dual-modal imaging capability of TCC@M was also in vitro characterized. Compared to Ti_3C_2, the PA spectrum of TCC@M exhibited a new peak at 680 nm (**Figure** 2A), which was attributed to the presence of Ce6 and was consistent with the absorption spectra (Figure 1B). The PA intensity of TCC@M at the same concentration of Ti_3C_2 decreased due to the presence of cell membrane coating, but was six times stronger than that of the water, making it suitable for PA imaging in vivo (Figure 2A). In order to demonstrate the effect of coating on the PA intensity, different thicknesses of chicken breast muscles were used to cover the polythene tubes filled with TCC@M solution, which showed gradually decreasing PA intensity with the increasing thicknesses (Figure 2B), and larger penetration depth under the irradiation of 780 nm than 680 nm (Figure S6, Supporting Information). When covering the polythene tube with 2 mm of chicken breast, the PA signal decreased by 50% at 680 nm, and only 20% at 780 nm. Considering the larger penetration depth and the effect of endogenous blood oxygen signal at 680 nm,[21] the in vivo PA imaging was performed with 780 nm excitation.

In addition to the PA imaging, thermal imaging is also an effective method for monitoring in vivo PTT efficacy. As expected, with the increasing irradiation time, power density or TCC@M concentration, the in vitro thermal imaging signal of TCC@M quickly enhanced and trended the maximum temperature (Figure 2C), indicating the thermal imaging capability of TCC@M.

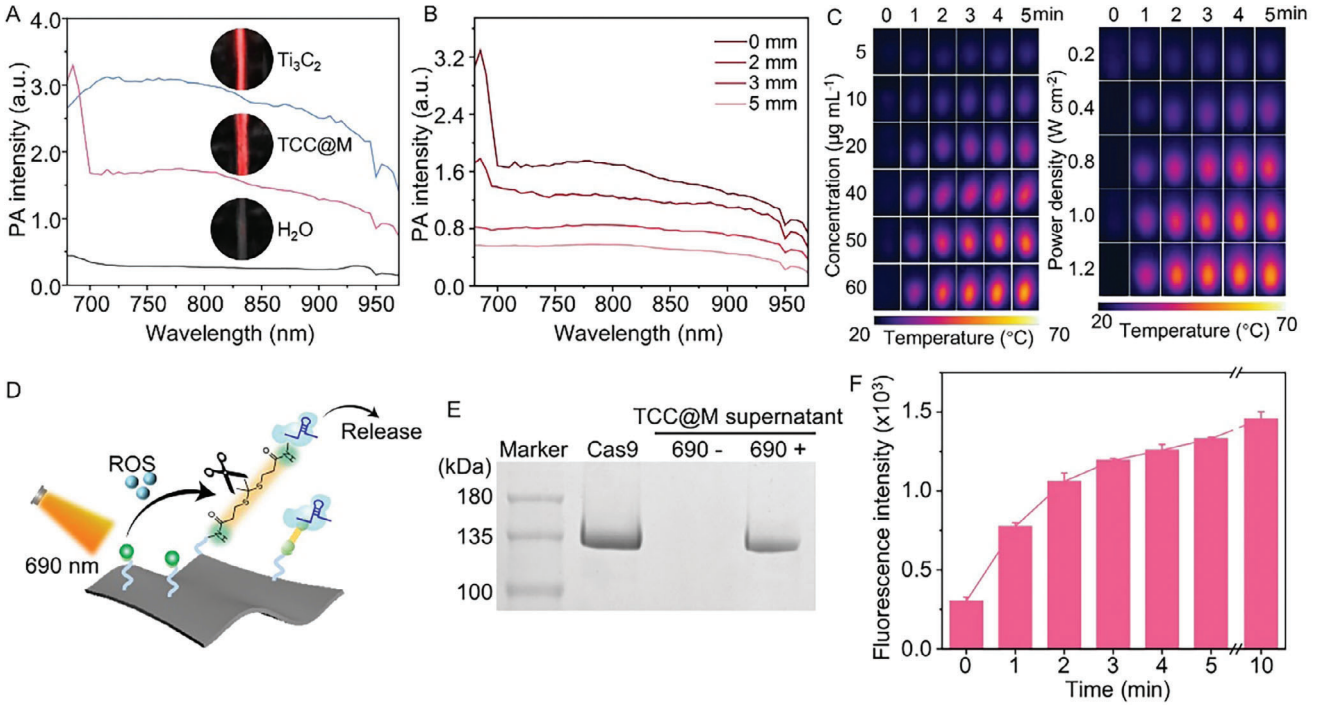

Figure 2. PA/thermal imaging of TCC@M and light–controlled release of Cas9 RNP. (A) PA spectra and images (inset) of water, Ti_3C_2 (200 μg mL^{-1}) and TCC@M solution containing 200 μg mL^{-1} Ti_3C_2. (B) PA spectra of TCC@M covered with chicken breast tissues at different thicknesses. (C) Thermal images of TCC@M at various concentrations (0.8 W cm^{-2}) and power densities (50 μg mL^{-1}) for different irradiation times. (D) Schematic illustration of Cas9 RNP release from TCC@M under 690 nm irradiation. (E) SDS-PAGE analysis of Cas9 protein and TCC@M supernatant after centrifugation with or without 690 nm irradiation. (F) Fluorescence intensity of the supernatant of FITC-Cas9 based TCC@M after 690 nm irradiation for different times at the excitation of 480 nm. The data error bars represent mean ± SD ($n = 3$).

2.2. Light–Controlled Release of Cas9 RNP

Upon 690 nm irradiation, the electron excitation of Ce6 induced the generation of singlet oxygen ($^1O_2$), a form of reactive oxygen species (ROS), from ground-state molecular oxygen ($^3O_2$),[22] which could cleave TK to release Cas9 RNP (Figure 2D). To verify $^1O_2$ generation, singlet oxygen sensor green fluorescent probe (SOSG) was added in TCC@M solution to expose to 690 nm irradiation, which led to $^1O_2$ responsive fluorescence decrease at 550 nm (Figure S7, Supporting Information). After TCC@M solution was exposed to 690 nm irradiation for 1 min, the supernatant showed an SDA-PAGE band as that of Cas9 protein, which did not occur in the absence of irradiation (Figure 2E), demonstrating the expected release of Cas9 RNP after photodynamic cleavage of TK. To further confirm the release of Cas9 RNP, FITC labeled Cas9 protein was used for the preparation of control TCC@M. The supernatant showed the increasing FL signal of FITC at 525 nm after exposed to 690 nm irradiation for increasing time (Figure 2F), demonstrating the efficient cleavage of TK to release Cas9 from TCC@M.

2.3. Cellular Uptake of TCC@M and Nuclei Entry of Cas9 RNP

After A549 cells were incubated with different concentrations of TCC@M, the cell viability did not obviously change, indicating that the TCC@M possessed good biocompatibility with negligible cytotoxicity even at a concentration of 100 μg mL^{-1} (Figure S8, Supporting Information), consistent with the previous report of membrane-enveloped nanoparticles.[23] At 50 μg mL^{-1} TCC@M prepared with FITC-labeled Cas9, the incubated A549 cells showed obviously enhanced fluorescence of both Ce6 and FITC with the prolonged incubation time, which occurred around nuclei stained with Hoechst 33 342 (Figure S9, Supporting Information), indicating the internalization of TCC@M into the lysosomes, which was demonstrated by the co-localization fluorescence of LysoTracker and Ce6 (Figure S10, Supporting Information). Obviously, TCC@M exhibited significantly higher internalization than TCC due to the presence of cell membranes, which enhanced the adhesion of homotypic cells by specifically recognizing molecules such as EpCAM, N-cadherin, and galectin-3[24] for targeting delivery (**Figure 3**A), leading to that more TCC@M were internalized into A549 cells than B16-F10 cells, Hela cells, and MCF-7 cells (Figure S11, Supporting Information).

To verify the endocytosis pathway of TCC@M, A549 cells were firstly treated with different endocytosis pathway inhibitors, such as ethylisopropylamiloride (EIPA, an inhibitor of macropinocytosis mediated endocytosis), nystatin (Nys, an inhibitor of caveolin-mediated endocytosis), and chlorpromazine hydrochloride (CPZ, an inhibitor of clathrin-mediated endocytosis) and then the TCC@M prepared with FITC-labeled Cas9. CPZ treatment resulted in a decrease of fluorescence signal by 36.6%, while EIPA and Nys did not show an obvious inhibition effect

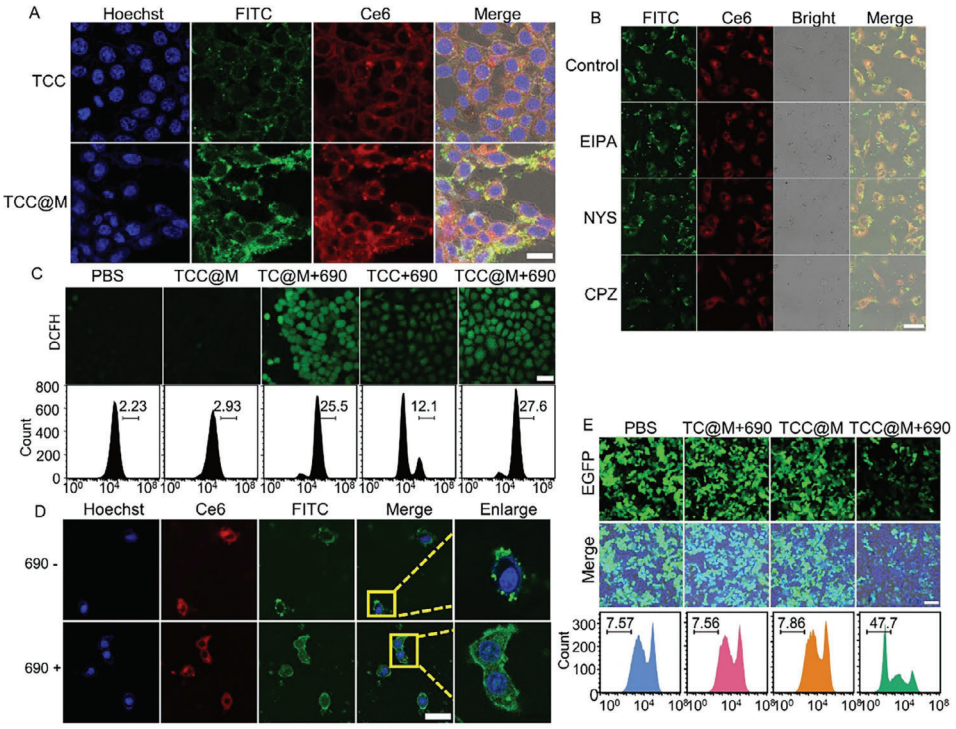

Figure 3. Cellular uptake and light-controlled release of Cas9 RNP in A549 cells. (A) CLSM images of A549 cells after incubated with FITC-Cas9 based TCC and TCC@M for 4 h. Scale bar, 20 μm. (B) CLSM images of A549 cells treated with EIPA, Nys or CPZ as endocytosis inhibitor and then incubated with 50 μg mL^{-1} TCC@M for 4 h. Green, FITC labeled Cas9 in TCC@M; red, Ce6 in TCC@M. Scale bar, 50 μm. (C) CLSM images and flow cytometric analysis of ROS levels in A549 cells with various treatments. Scale bar, 50 μm. (D) CLSM images of A549 cells incubated with TCC@M for 4 h with or without 690 nm irradiation. Scale bar, 50 μm. (E) CLSM images and flow cytometric analysis of TC@M or TCC@M treated EGFP-A549 cells with or without irradiation.

(Figure 3B), indicating that TCC@M was primarily internalized via clathrin-dependent endocytosis, generally referred to as "receptor-mediated endocytosis",[25] which further demonstrated the contribution of targeting delivery.

After TCC@M internalized A549 cells were incubated with ROS-detection agent DCFH-DA for 20 min and then exposed to 690 nm irradiation (40 mW cm^{-2}) for 1 min, both the CLSM image and flow cytometric assay of the A549 cells showed much stronger fluorescence of DCFH at 488 nm than TCC internalized A549 cells, and similar fluorescence to TC@M internalized cells, while the fluorescence of DCFH in the cells without 690 nm irradiation and the cells treated with only PBS was negligible (Figure 3C), indicating the generation of much more ROS in the presence cell membranes for targeting delivery, and the necessity of both 690 nm irradiation and photosensitizer Ce6 for generating the ROS.

The produced ROS could not only cleave TK to release Cas9 RNP, but also destabilize lysosome membranes to facilitate the rupture of lysosomal vesicles[26] for subsequent Cas9 RNP delivery into the nuclei. Thus the lysosomal rupture could be observed after 690 nm irradiation (Figure S10, Supporting Information), which showed decreased LysoTracker fluorescence and scattered Ce6 fluorescence due to the escape of TCC@M from lysosomes. After ROS-mediated cleavage of TK and release of Cas9 RNP, the green fluorescence of FITC labeled to Cas9 was observed in the nuclei (Figure 3D), while the cells without 690 nm irradiation did not show the green fluorescence in nuclei region, indicating the successful release and entrance of Cas9 RNP into nuclei directed by the fused nuclear localization sequence.

2.4. TCC@M–Mediated Gene Degrading and Apoptosis in A549 Cells

To verify the cleavage capability of Cas9 RNP delivered into nuclei to specific gene, an EGFP-targeting sgRNA was used for the preparation of Cas9 RNP and TCC@M, and the A549 cells stably expressing enhanced green fluorescent protein (EGFP-A549) were purchased to assess the gene degrading efficiency. After irradiating the TCC@M treated A549 cells under 690 nm for 1 min and then incubation for 48 h, a dramatic decrease in green fluorescence was observed, while other groups did not show observable change (Figure 3E), demonstrating the degradation of EGFP and the specific cleavage capability of Cas9 RNP. Flow cytometric analysis of the EGFP-negative cells showed EGFP knockout in ≈47.7% of the EGFP-A549 cells, whereas the knockout in other groups was negligible.

To achieve the enhanced PTT by effectively sensitizing cancer cells to heat, HSP90α gene knockout was performed to reduce the expression of HSP90α protein in the cells. Thus the sgRNA was designed to target HSP90α gene (**Figure** 4A). The targeting cleavage capability of the designed Cas9 RNP for

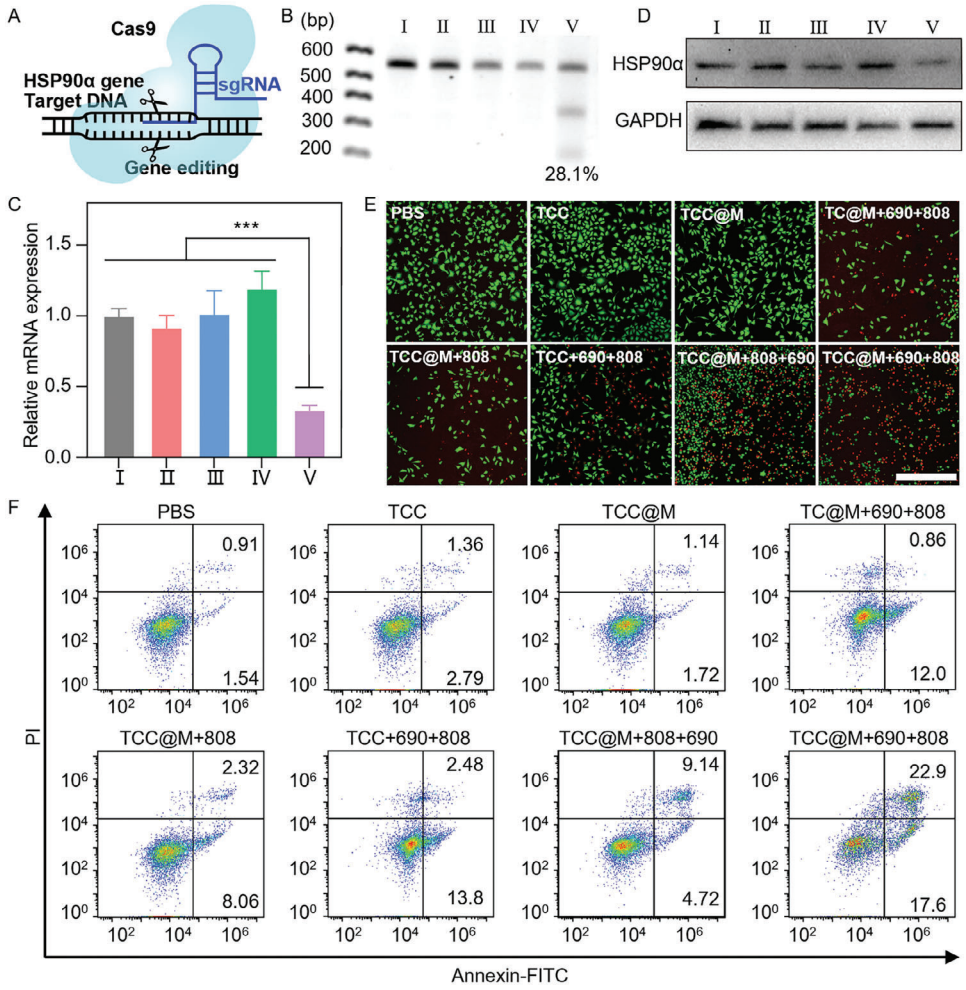

Figure 4. TCC@M–mediated gene degradation in A549 cells and apoptosis. (A) Schematic illustration of gene degradation mechanism. (B) T7E1 assay of indel frequencies of HSP90α DNA in A549 cells incubated with (I) PBS, (II) TC@M, (III) TCC@M, (IV, V) TCC@M after 808 nm (IV) or 690 nm (V) irradiation. (C) Western blotting analysis of HSP90α protein extracted from treated cells. (D) qRT-PCR analysis of relative HSP90α mRNA expression in treated cells ($^{***}p < 0.001$). (E) Fluorescent images of cells incubated with PBS, TCC, TC@M, and TCC@M with or without irradiation, and then stained with calcein AM/PI. Green: calcein AM; red, PI. Scale bar, 500 μm. (F) Flow cytometric assay of A549 cells after different treatments and then staining with Annexin V-FITC and PI.

degrading HSP90α gene was demonstrated by T7endonuclease I (T7E1) assay of the extracted HSP90α DNA from the TCC@M and then 690 nm irradiation treated A549 cells, which showed two new PAGE bands at lower molecular weight compared to other three kinds of TCC@M prepared with off-target sgRNAs (Figure S12, Supporting Information), showing the low off-target nature of Cas RNP.[27] Moreover, only the A549 cells treated with both the TCC@M and 690 nm irradiation showed these PAGE bands (Figure 4B), indicating the accessibility of light irradiation-controlled gene regulation. The gene cleavage efficiency under 1 min irradiation and then 48 h incubation was calculated to be 28.1%, which was close to the cleavage efficiency of 31.1% from another batch of measurements (Figure S12, Supporting Information), and thus led to significantly reduced HSP90α mRNA expression in the cells (Figure 4C). The degradation of HSP90α gene obviously decreased the amount of HSP90α protein in the cells (Figure 4D), thus resulted in lower cell viability of the treated A549 cells (Figure S13, Supporting Information), and more apoptosis of the A549 cells treated with TCC@M and 690+808 nm irradiations (Figure 4E,F), confirming the spatiotemporal precision of gene regulation and providing an enhanced PTT strategy.

2.5. In Vivo Multimodal Imaging for Optimizing Treatment Procedure

In vivo PA/FL/thermal imaging ability of the TCC@M were demonstrated by intravenously injecting 200 μL TCC@M solution (300 μg mL^{-1}) in A549 tumor-bearing nude mice. The whole-body FL images and the PA images at the tumor site with different time intervals were acquired post-injection. After injecting TCC@M the mice showed quickly increasing fluorescence of Ce6 in TCC@M at the tumor site (**Figure 5**A), which reached the maximum intensity at 4 h (Figure 5B), indicating the maximum accumulation of the TCC@M. Compared to TCC injection, TCC@M injection showed much stronger fluorescence at the same times

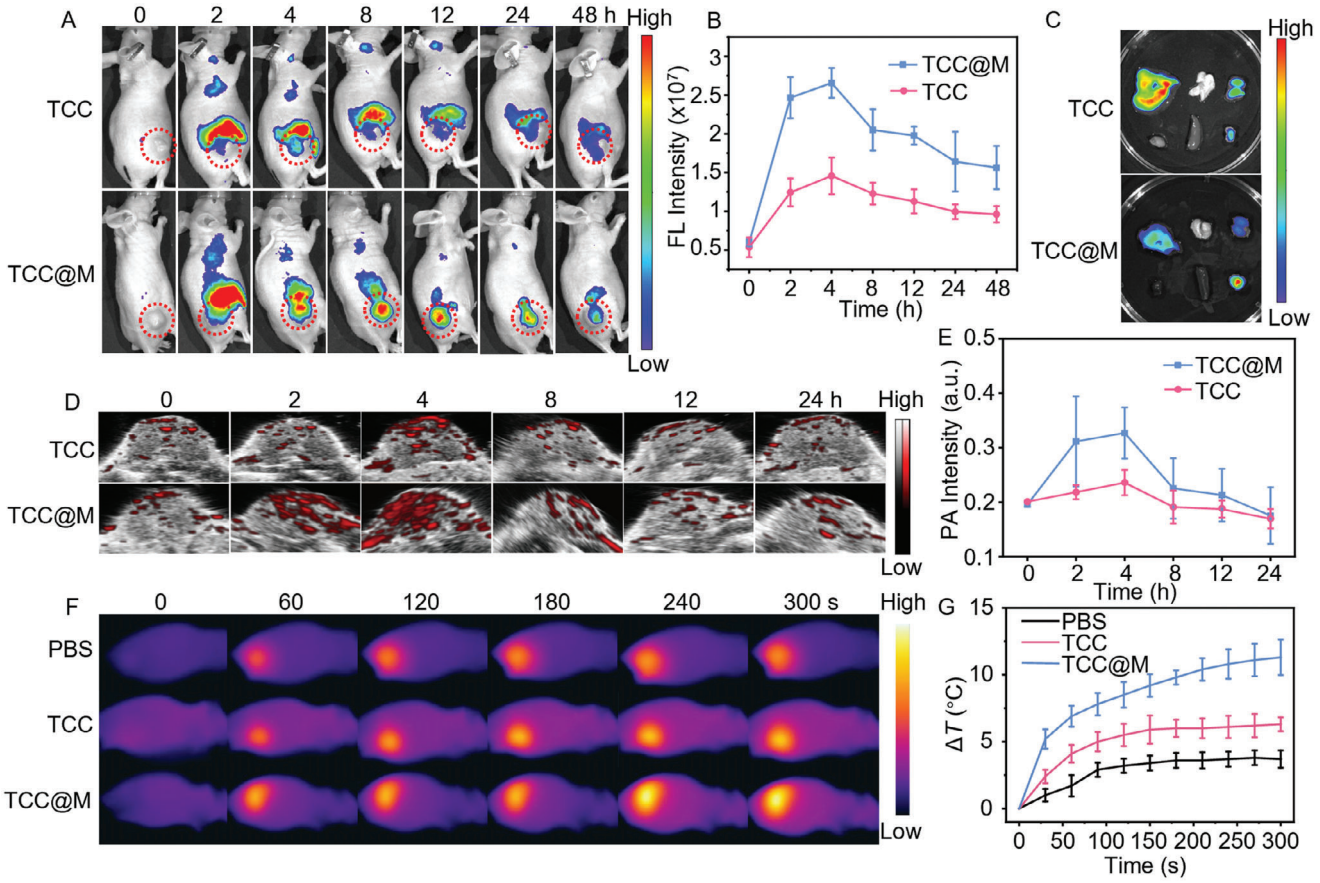

Figure 5. In vivo multimodal imaging. (A) FL images of A549 tumors after injecting TCC or TCC@M (300 μg mL^{-1}, 200 μL) for different times under *Ex*/*Em* of 660 nm/710 ± 20 nm. (B) Plot of FL intensity versus time in (A). (C) Ex vivo FL images of A549 tumors and major organs after injecting TCC or TCC@M for 48 h. (D) PA images (780 nm) and (E) intensities of A549 tumors after injecting TCC or TCC@M for different times. (F) Thermal images and (G) temperature changes of A549 tumors after injection PBS, TCC or TCC@M for 4 h and then 808 nm irradiation (1 W cm^{-2}) for different times. The error bars indicate mean ± SD ($n = 3$).

due to the targeting ability of cell membrane coating to the tumor site, which also resulted in higher background of TCC group. After post-injection for 4 h, the fluorescence gradually decreased due to TCC@M metabolism. Interestingly, TCC group showed much stronger fluorescence in liver than TCC@M group at 48 h post-injection (Figure 5C), indicating more TCC were accumulated in liver due to the lack of targeting groups. The same intensity changes were also observed from the PA images recorded by VEVO LAZR-X photoacoustic imaging system (Figure 5D,E). Both the imaging results showed the maximum accumulation of the TCC@M at the tumor site at 4 h after injection. Considering 92.3% accumulation amount of the TCC@M at 2 h after injection (Figure 5B) and subsequent delivery of Cas9 RNP into nuclei and CRISPR-Cas9 triggered degradation of HSP90*α* gene, following study selected 2 h after injection to perform the first irradiation under 690 nm for photodynamic release of Cas9 RNP.

The thermal imaging could be performed during the enhanced PTT by exposing the tumor sites of A549 tumor-bearing mice to 808 nm irradiation (1 W cm^{-2}), which showed time-dependent temperature change at tumor site (Figure 5F). With the increasing irradiation time the temperature at tumor site increased from 33.5 °C and then trended the maximum value (Figure 5G). After 5 min irradiation at an optimal power density of 1 W cm^{-2}, the temperature reached 44.8 °C, which was a mild temperature (<45 °C) for decreasing the damage of normal tissues surrounding the tumor,[7a] thus was selected as the optimal time for the second irradiation. From the thermal images, the PBS and TCC injected A549 tumor-bearing mice showed much slower temperature rise due to the lack of photothermal material at the tumor site.

2.6. TCC@M–Mediated PPT

The TCC@M–mediated PTT was performed using thirty BALB/c female nude mice with A549 xenografts, which were randomized into six groups and intravenously injected different formulations (200 μL) every three days with 690 nm irradiation (40 mW cm^{-2}) for 5 min and then 808 nm irradiation (1 W cm^{-2}) for 5 min (**Figure 6A**). The body weights of all mice did not apparently change in 14 days (Figure 6B), demonstrating the low toxicity of these formulations, which were consistent with hemolysis test and hematoxylin & eosin (H&E) staining of major organs except the liver with a little hepatoxicity after TCC and 690 + 808 nm

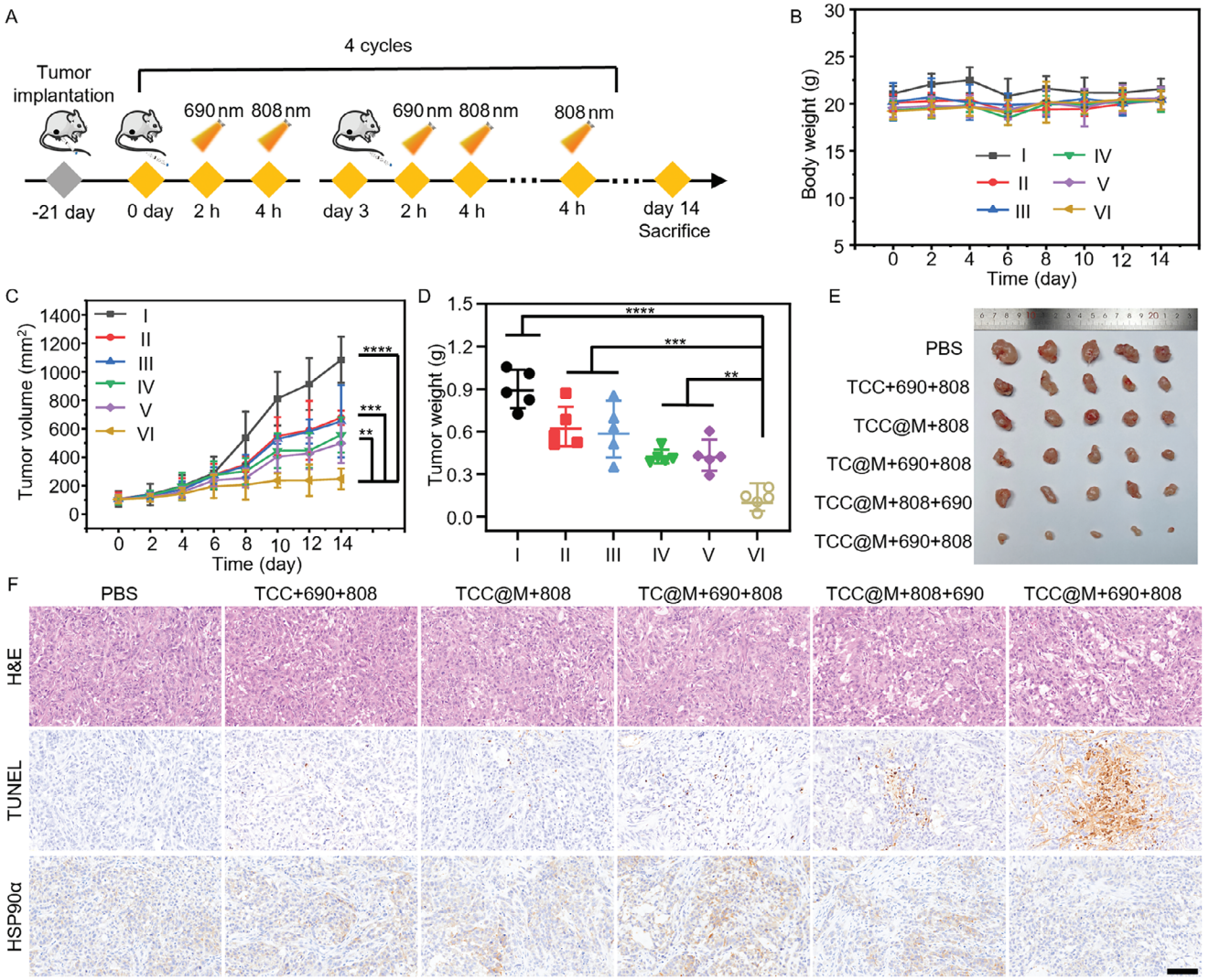

Figure 6. Light-controlled therapy of A549 tumor-bearing nude mice with TCC@M. (A) Schematic illustration of treatment process. (B) Time-dependent body weight of mice after injection with (I) PBS, (II) TCC and then 690 and 808 nm irradiation, (III) TCC@M and then 808 nm irradiation, (IV) TC@M and then 690 and 808 nm irradiation, (V) TCC@M and then 808 and 690 nm irradiation, and (VI) TCC@M and then 690 and 808 nm irradiation for 4 cycles ($n = 5$). (C–E) Tumor volumes (C), weights (D) and photographs of tumors (E) after different treatments ($n = 5$). $^{**}p < 0.01$, $^{***}p < 0.001$ and $^{****}p < 0.0001$. (F) Treated tumor tissues after H&E staining, TUNEL staining and HSP90α protein staining. Scale bar: 100 μm.

treatments (Figures S14 and S15, Supporting Information). During 4 cycles of treatments and post-treatments for 2 days, the tumor volume in PBS control group showed a tendency of rapid increase and the other control groups could not effectively inhibit tumor growth due to the heat resistance of HSPs (Figure 6C). Obviously, TCC@M and 690 + 808 nm irradiations treated mice exhibited the highest tumor suppression both in tumor volume and tumor weight (Figure 6D), which were further verified from the photographs of dissected tumors (Figure 6E) and could be attributed to the knockout of HSP90α gene by Cas9 RNP prior to PTT. Notably, the skin of mice did not show obvious damage due to the gene regulation-enhanced PTT at mild temperature (<45 °C) (Figure S16, Supporting Information).

The treated tumor tissues were further studied by H&E staining and TdT-mediated dUTP nick-end labeling (TUNEL). TCC@M+690+808 group showed the largest necrotic area and the most apoptotic cells (Figure 6F), confirming the enhanced PTT due to the downregulation of HSP90α protein in the tumor tissues, which was demonstrated with immunohistochemistry (IHC) and Western blotting analysis (Figures 6F and S17A, Supporting Information). HSP90α mRNA and DNA in the tumor were also extracted and analyzed with qPCR and T7E1 assay, which showed a DNA cleavage efficiency of 11.6% and the similar results to protein expression (Figure S17B,C, Supporting Information) and cell experiments (Figure 4B,C), and demonstrated the designed mechanism for enhanced PTT.

3. Conclusion

In conclusion, this work has developed a gene regulation-enhanced PTT mechanism by sequentially activating biofunctional MXenes to release Cas9 RNP and CRISPR-Cas9 triggered

degradation of HSP90α gene followed by PTT. The biofunctional MXenes can be conveniently prepared by binding Ce6 and then Cas9 RNP to Ti_3C_2 NSs and enveloping the modified NSs with cell membranes for targeting delivery. The gene regulation can be performed in cancer cells or tumor by 690 nm irradiation of internalized TCC@M to achieve photodynamic cleavage of TK for releasing Cas9 RNP, which enters the nuclei by the fused nuclear localization sequence in Cas9 to specifically cleave HSP90α DNA, leading to the reduce of HSP90α protein expression, and thus sensitizing cancer cells to heat. The enhanced PTT can be performed at a mild temperature (<45 °C) by 808 nm irradiation with a relatively time, which greatly decreasing the damage of normal tissues during PTT. More importantly, the designed TCC@M achieves FL/PA/thermal multimodal imaging for optimizing the treatment procedure and guiding the irradiations, realizing the spatiotemporal controllability of PTT and precision therapy of cancer.

Supporting Information

Supporting Information is available from the Wiley Online Library or from the author.

Acknowledgements

J.J. and X.Z. contributed equally to this work. This work was financially supported by National Natural Science Foundation of China (21890741).

Conflict of Interest

The authors declare no conflict of interest.

Data Availability Statement

The data that support the findings of this study are available from the corresponding author upon reasonable request.

Keywords

biofunctional MXenes, CRISPR-Cas9, MXenes, photothermal therapy, sequential activation

Received: November 7, 2024
Revised: November 26, 2024
Published online:

[1] a) W. Fan, B. Yung, P. Huang, X. Chen, *Chem. Rev.* **2017**, *117*, 13566; b) L. Fu, C. Qi, Y. Hu, J. Lin, P. Huang, *Adv. Mater.* **2019**, *31*, 1808325.
[2] a) G. Shim, M.-G. Kim, D. Kim, J. Y. Park, Y.-K. Oh, *Adv. Drug. Delivery. Rev.* **2017**, *115*, 57; b) Z. Wei, E. Volkova, M. R. Blatchley, S. Gerecht, *Adv. Drug. Delivery. Rev.* **2019**, *149–150*, 95.
[3] a) A. Zakharchenko, N. Guz, A. M. Laradji, E. Katz, S. Minko, *Nat. Catal.* **2018**, *1*, 73; b) H. P. Lee, A. K. Gaharwar, *Adv. Sci.* **2020**, *7*, 2000863; c) Y. Duan, Y. Yu, P. Liu, Y. Gao, X. Dai, L. Zhang, L. Chen, Y. Chen, *Angew. Chem., Int. Ed.* **2023**, *62*, 202302146.
[4] a) X. Li, Y. Pan, C. Chen, Y. Gao, X. Liu, K. Yang, X. Luan, D. Zhou, F. Zeng, X. Han, Y. Song, *Angew. Chem., Int. Ed.* **2021**, *60*, 21200; b) K. Zhu, S. Qian, H. Guo, Q. Wang, X. Chu, X. Wang, S. Lu, Y. Peng, Y. Guo, Z. Zhu, T. Qin, B. Liu, Y. Yang, B. Wang, *ACS Nano* **2022**, *16*, 11136; c) Q. Wang, X. Li, J. Mao, X. Qin, S. Yang, J. Hao, M. Guan, Y. Cao, Y. Li, *Adv. Healthcare. Mater.* **2022**, *11*, 2101634.
[5] a) J. Yan, X. Ma, D. Liang, M. Ran, D. Zheng, X. Chen, S. Zhou, W. Sun, X. Shen, H. Zhang, *Nat. Commun.* **2023**, *14*, 6905; b) Q. T. Hoang, D. Y. Kim, H. S. Park, W. Jang, T. G. Nguyen Cao, J. H. Kang, Y. T. Ko, S. J. Mun, S. H. Bhang, M. S. Shim, K. W. Bong, *Adv. Funct. Mater.* **2024**, *34*, 2306078; c) S. Zhang, Y. Lai, J. Pan, M. Saeed, S. Li, H. Zhou, X. Jiang, J. Gao, Y. Zhu, H. Yu, W. Zhang, Z. Xu, *Adv. Mater.* **2024**, *36*, 2314132.
[6] S. Diamant, P. Goloubinoff, *Biochemistry* **1998**, *37*, 9688.
[7] a) G. Gao, Y. Jiang, W. Sun, Y. Guo, H. Jia, X. Yu, G. Pan, F. Wu, *Small* **2019**, *15*, 1900501; b) Z. Chen, S. Li, F. Li, C. Qin, X. Li, G. Qing, J. Wang, B. Xia, F. Zhang, L. Meng, X. Liang, Y. Xiao, *Adv. Sci.* **2023**, *10*, 2206707; c) Q. Yu, J. Zhou, H. Wang, Y. Liu, H. Zhou, B. Kang, H. Chen, J. Xu, *Chem. Biomed. Imaging* **2023**, *1*, 242.
[8] a) S. Bi, W. Chen, Y. Fang, J. Shen, Q. Zhang, H. Guo, H. Ju, Y. Liu, *Angew. Chem., Int. Ed.* **2024**, *63*, 202402522; b) R. J. Sullivan, J. S. Weber, *Nat. Rev. Drug Discovery* **2022**, *21*, 495.
[9] a) O. Genest, S. Wickner, S. M. Doyle, *J. Biol. Chem.* **2019**, *294*, 2109; b) R. Rosenzweig, N. B. Nillegoda, M. P. Mayer, B. Bukau, *Nat. Rev. Mol. Cell Biol.* **2019**, *20*, 665.
[10] a) H. Liao, S. Wang, X. Wang, Z. Dai, Y. Zhang, C. Zhu, J. Li, *Chem. Biomed. Imaging* **2024**, *2*, 313; b) B. Li, E. Pang, S. Zhao, G. Deng, S. Wang, B. Wang, J. Wu, G. Niu, X. Song, M. Lan, *Chem. Biomed. Imaging* **2023**, *1*, 541; c) Q. Wang, H. Yang, Y. Liu, Z. Zhou, X. Zhang, M. Sang, F. Xu, L. Song, T. Xia, Y. Zhang, J. Wei, X. Zhang, Q. Ding, *Adv. Healthcare. Mater.* **2023**, *12*, 2300420.
[11] a) N. Ankenbruck, T. Courtney, Y. Naro, A. Deiters, *Angew. Chem., Int. Ed.* **2018**, *57*, 2768; b) Y. Zhou, D. Kong, X. Wang, G. Yu, X. Wu, N. Guan, W. Weber, H. Ye, *Nat. Biotechnol.* **2022**, *40*, 262.
[12] a) Y. Li, Y. Xie, Y. Zhang, H. Zhao, H. Ju, Y. Liu, *Anal. Chim. Acta* **2022**, *1221*, 340149; b) C. Wang, Y. Xie, X. Song, Z. Chao, K. Wu, Y. Fang, H. Zhao, H. Ju, Y. Liu, *Angew. Chem., Int. Ed.* **2023**, *62*, 202312665.
[13] a) C. Tan, X. Cao, X. Wu, Q. He, J. Yang, X. Zhang, J. Chen, W. Zhao, S. Han, G.-H. Nam, M. Sindoro, H. Zhang, *Chem. Rev.* **2017**, *117*, 6225; b) N. Li, Y. Wang, Y. Li, C. Zhang, G. Fang, *Small* **2024**, *20*, 2305645.
[14] a) F. Gao, C. Xue, T. Zhang, L. Zhang, G. Zhu, C. Ou, Y. Zhang, X. Dong, *Adv. Mater.* **2023**, *35*, 2302559; b) R. Zhao, Y. Zhu, L. Feng, B. Liu, Y. Hu, H. Zhu, Z. Zhao, H. Ding, S. Gai, P. Yang, *Adv. Mater.* **2024**, *36*, 2307115.
[15] a) X. Ge, H. Cui, J. Kong, S. Lu, R. Zhan, J. Gao, Y. Xu, S. Lin, K. Meng, L. Zu, S. Guo, L. Zheng, *Adv. Mater.* **2020**, *32*, 2000037; b) Y. Zhu, Z. Wang, R. Zhao, Y. Zhou, L. Feng, S. Gai, P. Yang, *ACS Nano* **2022**, *16*, 3105.
[16] a) K. Lee, M. Conboy, H. M. Park, F. Jiang, H. J. Kim, M. A. Dewitt, V. A. Mackley, K. Chang, A. Rao, C. Skinner, T. Shobha, M. Mehdipour, H. Liu, W.-c. Huang, F. Lan, N. L. Bray, S. Li, J. E. Corn, K. Kataoka, J. A. Doudna, I. Conboy, N. Murthy, *Nat. Biomed. Eng.* **2017**, *1*, 889; b) V. Madigan, F. Zhang, J. E. Dahlman, *Nat. Rev. Drug Discovery* **2023**, *22*, 875; c) X. Yan, Q. Pan, H. Xin, Y. Chen, Y. Ping, *Sci. Adv.* **2021**, *7*, eabj0624; d) W. Cai, T. Luo, L. Mao, M. Wang, *Angew. Chem., Int. Ed.* **2021**, *60*, 8596.
[17] a) P. Dash, A. M. Piras, M. Dash, *J. Controlled. Release.* **2020**, *327*, 546; b) N. Krishnan, R. H. Fang, L. Zhang, *Adv. Drug. Delivery. Rev.* **2021**, *179*, 114006; c) B. Rezaei, A. Harun, X. Wu, P. R. Iyer, S. Mostufa, S. Ciannella, I. H. Karampelas, J. Chalmers, I. Srivastava, J. Gómez-Pastora, K. Wu, *Adv. Healthcare. Mater.* **2024**, *13*, 2401213.
[18] C. Backes, T. M. Higgins, A. Kelly, C. Boland, A. Harvey, D. Hanlon, J. N. Coleman, *Chem. Mater.* **2017**, *29*, 243.

[19] Z. Li, H. Zhang, J. Han, Y. Chen, H. Lin, T. Yang, *Adv. Mater.* **2018**, *30*, 1706981.
[20] H. Lin, X. Wang, L. Yu, Y. Chen, J. Shi, *Nano Lett.* **2017**, *17*, 384.
[21] Y. P. Xiao, P. H. Chen, S. Lei, F. Bai, L. H. Fu, J. Lin, P. Huang, *Angew. Chem., Int. Ed.* **2022**, *61*, 202204584.
[22] S. Deng, X. Li, S. Liu, J. Chen, M. Li, S. Y. Chew, K. W. Leong, D. Cheng, *Sci. Adv.* **2020**, *6*, eabb4005.
[23] L. He, T. Nie, X. Xia, T. Liu, Y. Huang, X. Wang, T. Chen, *Adv. Funct. Mater.* **2019**, *29*, 1901240.
[24] a) H. Sun, J. Su, Q. Meng, Q. Yin, L. Chen, W. Gu, P. Zhang, Z. Zhang, H. Yu, S. Wang, Y. Li, *Adv. Mater.* **2016**, *28*, 9581; b) J. Zhu, C. Sevencan, M. Zhang, R. S. A. McCoy, X. Ding, J. Ye, J. Xie, K. Ariga, J. Feng, B. H. Bay, D. T. Leong, *ACS Nano* **2020**, *14*, 3259.
[25] a) S. Xu, B. Z. Olenyuk, C. T. Okamoto, S. F. Hamm-Alvarez, *Adv. Drug. Delivery. Rev.* **2013**, *65*, 121; b) L. Liu, X. Bai, M.-V. Martikainen, A. Kårlund, M. Roponen, W. Xu, G. Hu, E. Tasciotti, V.-P. Lehto, *Nat. Commun.* **2021**, *12*, 5726.
[26] a) Y. Zhang, K. Ren, X. Zhang, Z. Chao, Y. Yang, D. Ye, Z. Dai, Y. Liu, H. Ju, *Biomaterials* **2018**, *163*, 55; b) W. Chen, H. He, P. Jiao, L. Han, J. Li, X. Wang, X. Guo, *Adv. Healthcare. Mater.* **2023**, *12*, 2301785.
[27] a) H. X. Wang, M. Li, C. M. Lee, S. Chakraborty, H.-W. Kim, G. Bao, K. W. Leong, *Chem. Rev.* **2017**, *117*, 9874; b) Y. Q. Lin, K. K. Feng, J. Y. Lu, J. Q. Le, W. L. Li, B. C. Zhang, C. L. Li, X. H. Song, L. W. Tong, J. W. Shao, *J. Controlled. Release.* **2023**, *361*, 727.